Microstructural and mechanical analysis on Cu-Sn intermetallic micro-joints under isothermal condition

L. Mo [a, b], Z. Chen [a, b], F. Wu [a, *], C. Liu [b, *]

[a] State Key Laboratory of Material Processing and Die & Mould Technology, Huazhong University of Science and Technology, Wuhan, 430074, China.

[b] Wolfson School of Mechanical and Manufacturing Engineering, Loughborough University, Loughborough, LE11 3TU, UK.

* Corresponding author E-mail address: fengshunwu@hust.edu.cn, C.Liu@lboro.ac.uk

Abstract

This study focuses on the mechanism of phase transformation from Cu_6Sn_5 into Cu_3Sn and the homogenization process in full intermetallics (IMCs) micro-joints, which were prepared by soldering the initial Cu/Sn/Cu structure through high temperature storage in vacuum environment as the Transient Liquid Phase (TLP) process. From the microstructural observation by electron backscatter diffraction (EBSD), a mixture of IMCs phases (Cu_6Sn_5 and Cu_3Sn) has been found to constitute the sandwich-structured Cu/IMCs/Cu joints. With the dwell time increasing at 533K, there were two layers of Cu_3Sn emerging from both sides of copper substrates with the depletion of Cu_6Sn_5 layer, toward merging each other in the IMCs interlayer. Then the Cu_3Sn grains with various sizes became more homogenous columnar crystallites. Meanwhile, some equiaxial ultra-fine grains accompanied with the Kirkendall voids, were found only in adjacent to the electroplated copper. In addition, a specific type of micropillar with the size ~5μm×5μm×12μm fabricated by focus ion beam (FIB) was used to carry out the mechanical testing by Nano-indentation, which confirmed that this type of joint is mechanically robust, regardless of its porous Cu_3Sn IMC interconnection.

Keywords:

A. Intermetallics

B. Phase transformation, Grain boundary diffusion

F. Electron backscatter diffraction, Nanoindentation

1. Introduction

The packaging and integration using micro-bumps to connect the Through-Si-Vias (TSVs) chips in vertical direction are often required distinctive features from the conventional package formats. And, ensuring the reliability of these micro-joints (<10μm) has become one of the major challenges in the 3D integration [1-3]. Sn or Sn-based solder may be completely consumed with the scaling down size of joints during the stacking process, to form the entire intermetallic compounds (IMCs) interconnection. The formation and microstructural evolution of the solder joints at a relative large scale (e.g. >50μm) during the reflow and thermal aging process have been well studied [4-6]; however, further investigations are still needed to establish on the full IMCs interconnection without existence of any remnant solders, in particular, the discontinuity that are associated with the crystallite microstructure and mechanical integrity.

Thermal-compression process is commonly used to realize such miniaturized interconnections, instead of reflow utilized in conventional electronic packaging. The typical description of the metallurgical reaction during this soldering process is Solid-Liquid Interdiffusion (SLID) bonding [7-8] or Transient Liquid Phase (TLP) soldering [9-10]. As reported by references [11-12], the effect of process parameters (such as time, temperature, and pressure) on the microstructure of IMC joints can be significant which requires a further understanding as far as the reliability is concerned. And also, the minimum thickness of initial solder layer needed to form a pore-free joint has also been discussed in Bosco's paper [13], where at least 10μm of initial Sn layer was suggested. However the estimation was primarily based on the growth of the Cu_6Sn_5 grain without considering the growth of Cu_3Sn, thereby unsuitable for the case where the Sn layer is even thinner than 10μm and the growth of Cu_3Sn layer can be comparable against the Cu_6Sn_5 layer.

However, due to the further reduction of joint size, not only the manufacturing process of the IMC joints, but also the reliability of such formed joints are to be concerned ever more,. For instance, Kirkendall voids are normally found in Cu_3Sn layer or near the interface between Cu_3Sn and plated Cu substrate after aging or during the service period [14-16], which will strongly impact the reliability of the IMC interconnections. Besides, the IMCs are considered to be brittle since the cleavage morphology is often observed at the IMC

fractured surfaces. Ghosh et al [17] have microscopically seen some slip bands appeared in Cu_3Sn during the indention test, which indicates the question whether the IMC is really brittle or not is still debatable [18]. Nevertheless, the electrical and mechanical properties of IMC joints will be governed by the characteristics of IMC layer significantly, since the IMCs are the only connected media in the Cu/IMCs/Cu joints. Therefore, in order to achieve the reliable miniaturized interconnections for 3D stacking of IMCs, the crystallites features of Cu-Sn IMCs and the effect of growth process including the transformation between different IMC phases and morphological evolution of IMCs are yet to be well understood. In this work, EBSD was selected to observe the microstructural change with phase transformation from Cu_6Sn_5 into Cu_3Sn IMCs, and the homogenization process in the entire Cu_3Sn IMC joints.

2. Experimental details

2.1 Preparation of Cu/IMCs/Cu test structure

In this study, polycrystalline oxygen-free rolled copper (20mm×15mm×1mm) was employed as substrate. A thin layer of Sn approximately 2.5μm thick was first electroplated on the substrate after pre-treatment of acid washing process, then a copper layer of ~10 μm was electroplated on the top of the plated Sn to create an initial Cu/Sn/Cu sandwich test structure, as shown in Fig. 1(a). Such sandwich structure was heated up to 533±1 K to allow Sn melting and reacting with surrounding Cu in a vacuum chamber with 93KPa absolute pressure, and followed by an isothermal storage process with different dwell time (10, 30, 50, 70 minutes). Finally, the specimens were removed from the vacuum chamber and cooled down to room temperature (R.T.) in air. This soldering process can also be described as TLP method.

2.2 Phase identification and EBSD analysis of IMCs

The type of IMCs phases was identified by X-ray diffraction (XRD-7000s, Shimadzu, Japan). The top Cu layer was removed by polishing to expose the IMCs interlayer as illustrated in Fig.1 (b). After this, the XRD detection with a copper target was conducted in the top view at 40KV, 30mA and 3deg/min to obtain the spectrum, and by following the indexing procedure the Cu_6Sn_5 and Cu_3Sn phases can be identified using MDI/Jade6 software supplied with the XRD machine.

In order to observe the microstructure of the Cu/IMCs/Cu interconnections at crystallite level, the cross-sections of specimens were further prepared by focus ion beam (FIB, FEI-Nova 600 Nanolab Dual Beam)

after general grinding and polishing process, then analyzed by EBSD module installed in the system in details. As the IMCs formed under high temperature with a long dwell time, thus both the Cu_6Sn_5 and Cu_3Sn are hexagonal structure [19, 20]. To facilitate the EBSD characterization, the Orientation Imaging Microscopy (OIM) software was utilized to collect the data with a 30 KV beam. The Image Quality (IQ) quick map and Phase Quick map were also plotted using OIM Analysis software to observe the microstructure and the phase distribution of joints. Inverse Pole Figure [001] (IPF) quick map and the discrete IPF of Cu_3Sn were also derived to display the orientation distribution of Cu_3Sn grains in micro-joints with 70mins dwell time. In addition, the phase ratios of each phase, the distribution of misorientation angle and grain size were estimated from the selected IMCs interlayers. Moreover, grain shape orientation (GSO) map referrng to the angle of the major axis from the horizontal, where the shape of grains can be fitted by ellipses, was also obtained from the OIM Analysis software to gain the evolution trend of Cu_3Sn grain shape with the prolonged dwell time.

2.3 Micro-mechanical testing

Mechanical testing was conducted by Nano-indentation machine (Micro Materials Nano Test600, UK) on the sample with dwell time of 70 mins. Firstly, a micropillar of ~5μm×5μm cross-sectional area was fabricated by FIB from Cu_3Sn IMC with voids included, as shown in Fig.2 (a). Secondly, a flat diamond indenter with diameter of 5μm was used to shear the micropillar completely, aiming at the Cu_3Sn layer as shown in Fig. 2(b). The loading rate of 0.05mN/s was applied in the shearing until the fracture occurred. Finally, the fracture surfaces were observed using field emission gun-scanning electron microscope (FEG-SEM, Carl Zeiss (Leo)-1530VP).

3. Results and discussion

3.1 EBSD analysis of Cu/IMCs/Cu interconnection

The microsturcture and phase distribution on Cu/IMCs/Cu cross-section from the samples reflowed at temperature of 533K for 10 minutes and 30 minutes are depicted in Fig. 3 and Fig. 4, respectively. From the IQ map, the shapes and number of IMC grains consisting of Cu_6Sn_5 and Cu_3Sn are revealed in details. Obviously, the entire IMCs interlayer can be divided into two sub-layers mainly composed of Cu_3Sn, growing and emerging from the two opposite sides of copper base with small amount of remanent Cu_6Sn_5

in the middle. It is worth noticing that a special layer contains some ultra-fine equiaxial Cu_3Sn grains accompanied with micro-voids as seen in Fig. 3 (a), which has also been reported by other researchers [21-23]. This layer is only found in adjacent to the electroplated copper, but does not appear on the opposite side of the initial rolled copper substrate.

With dwell time increasing, the Cu_6Sn_5 grains disappeared gradually, and the residual Cu_6Sn_5 phase surrounding the coarse Cu_3Sn phase still remained in Fig. 3 (b), Fig. 4 (b) and Fig. 5 (b). This does not agree with the layer by layer growth of IMCs in conventional soldering joints [9]. The XRD result demonstrated in Fig. 6(a) also confirms that the Cu_6Sn_5 phase still existed in the IMCs interlayer, even in the sample after 70 minutes dwelling. Furthermore, the ratio of each phase (Cu, Cu_6Sn_5 and Cu_3Sn) directly obtained from OIM Analysis software is plotted in Fig. 6 (b). Accordingly, the ratio of Cu_3Sn increased dramatically in the region of IMCs mixture as dwell time increased from 10 to 50 minutes. The Cu_3Sn phase can reach approximately 85% in the IMCs layer after 50 minutes, and this remained almost the same level with further increase of dwell time up to 70 mins.

The grain orientation of IMC interlayer is displayed by IPF map (Fig. 5 c) of the sample with 70 mins dwell time, where the different colors represent different orientations of grains. The result indicates that IMC layers near the both side of copper did not exhibit any obvious preferential orientations, although the rolled Cu substrate can be locally treated as single crystal. Also, in Fig. 5 (d), the randomly distributed black dots in the discrete IPF of Cu_3Sn IMC means no certain grain orientation preference that can be manifested in the Cu_3Sn IMC growth process even after dwelling for 70 mins, as has been reported elsewhere [19]. However, Zhang's work showed preferred orientation (100) of Cu_3Sn grains in parallel with copper substrate [24]. This may be due to the formation temperature of Cu_3Sn IMC layer in this study which is relatively lower than the temperature (573K) used in the Zhang's work, can cause the incomplete process of coarsening and homogenization.

3.2 Kinetic analysis on IMC grains in micro-joints

As the most Cu_6Sn_5 layer disappeared in the micro-joint within 10 minutes dwelling time, the subsequent homogenizing process of the IMCs interlayer took place with further prolonged dwell time, which caused the increase of grain size during the ripening process. Lifshitz-Slezov-Wahner (LSW) theory [25] was

established to describe the homogenizing process based on the diffusive decomposition in the supersaturated solid solutions, known as the classic Ostwald ripening process through decreasing the interfacial energy between phases in a conservative system. Another Flux-driven ripening (FDR) [26] theory was also developed later to describe the Cu_6Sn_5 ripening process during Cu-Sn solid-liquid reaction, where the growth and ripening of scallop-type Cu_6Sn_5 grains occurred simultaneously. In FDR theory, it is assumed that the Cu atoms diffused from the Cu substrate only lead to the growth of hemispheric Cu_6Sn_5, without considering the Cu_3Sn. The FDR was usually conducted in an open system, thus the volume of IMC layer increased while the surface energy of phase was thought to be consistent, which is different with the LSW theory.

Fig. 7 illustrates the distribution of normalized grain sizes of IMC (R/Ra, R-radius of grain, Ra-the average value of grain radius) as a function of dwell time. After dwelling 10 minutes, the mean value of grain size is approximately 0.26μm. And the random distribution of grain size deviates from the average value (Ra) significantly as shown in Fig. 7 (a) and (b). With the increase of dwell time, the mean value of IMC grain size increases and becomes larger than 0.5μm after 50 minutes or longer. The diameters of grains are expected to be linear with the cube-root of annealing time ($\sim t^{1/3}$), which is likely to obey the LSW theory of ripening, but this phenomenon herein is more probably characterized by the FDR theory. Although no liquid tin phase is involved in the full IMCs micro-joints during phase transformation process discussed here, the reaction such as $Cu_6Sn_5 + 9Cu \rightarrow 5Cu_3Sn$ is expected to take place throughout the dwelling period. Thus, both processes of growth and ripening have occurred simultaneously in the IMCs interlayer. In particular, copper atoms diffused through grain boundaries are mainly from copper substrate as a flux resource into IMCs layer during the whole evolution process. Therefore, the microstructural evolution of IMCs interlayer is predominantly controlled by diffusion of Cu atoms at the interface and almost grain boundaries where the samples were kept for a long time, the distribution of normalized grain sizes tends to be regular, which is similar to the FDR distribution based on Gusak's work [26], as shown in Fig. 7 (c) and (d). This means the microstructure of IMCs interlayer became much more stable and homogeneous in micro-joints after 50mins or longer dwell time.

The further analysis on the characteristics of IMCs grains was proceeded, and the morphologies of the IMC interlayer in both IQ map and GSO map are showed in Fig. 8 for the specimens dwelled for 50 and 70 minutes, respectively. The values of angles are represented by different colors in Fig. 8 (b) and (d). The light green and yellow represent those grains with shape angles around 90 degrees, which are perpendicular to the copper substrates. It is apparent that the ratio of the amount of those certain grains in Cu_3Sn IMC interlayer after 70min dwelling is higher than that after 50min. Besides, Fig. 9 shows the statistical results of misorientation distribution from experimental observation which measures number fraction of the grain boundaries with certain misorientation. Obviously, the low-misorientation grains boundaries are predominant within Cu_3Sn IMC for the samples with dwell time of 50 mins and 70mins. Based on the analysis in reference [27], the misorientation distribution is primarily concentrated on small misorientation, so the grains tend to be clustered. Therefore, the Cu_3Sn IMC grains have a great tendency to grow along the vertical direction on copper substrates with the increasing of dwell time.

3.3 Mechanism of microstructural evolution in the IMCs micro-joints

The major characteristics of SLID or TLP method used for soldering can be explained from the following two aspects: (1) the soldering temperature is constant and higher than the melting point of Sn-based solder alloy, leading the solder to becoming liquid phase at the first stage. As a consequence, Cu atoms will be uniformly distributed in the liquid Sn-based solder since a relative higher diffusion ratio of Cu atoms in the liquid solder than solid. (2) The liquid Sn solution will be saturated with copper atoms in a few minutes. Because of the higher melting temperature of the newly formed IMCs, the solidification stage is expected to occur even under the high temperature where the entire solder solution may still remain in a liquid condition, without need of a cooling process. Fig. 10 reveals the microstructure of Cu_6Sn_5 IMC layer in the sample with initial structure as Cu/ Sn (5μm) /Cu soldered by TLP method for 30min dwell time at 533K in vacuum chamber. The Cu_6Sn_5 grains varied and distributed irregularly, especially the ones in the middle or across the whole Cu_6Sn_5 layer appear like columnar grain as highlighted. Thus, when the interconnecting distance of the joint is less than 5μm, the formation of IMC micro-joints can be articulated as follows: (1) the nucleation and growth of grains will happen simultaneously and quickly in the saturated Sn liquid solution. (2) The neighboring grains appeared at the same time, so no time left for each grain growing up as a column. Then, the Cu_6Sn_5 layer with equiaxial grains formed in the middle of joints.

Therefore, the IMCs microstructure which is evolving with dwell time can be considered as Fig. 11 (a-f), concerning at grain level systematically. First of all, due to the very thin interconnected thickness, the sandwich IMCs joint structure consisting of Cu/Cu_3Sn/Cu_6Sn_5/Cu_3Sn /Cu tends to be formed after TLP soldering as shown in Fig. 11 (a). And the Cu_6Sn_5 grains are always larger than Cu_3Sn grains resulted from the Cu-Sn reaction. However, such joint structure is relatively unstable for the existence of Cu_6Sn_5 layer. At the interface close to Cu substrate, the concentration gradient and chemical reaction driving force cause the Cu atoms flux to diffuse from copper substrates into IMCs layer, as such the phase transformation of Cu_6Sn_5 into Cu_3Sn continues (Cu_6Sn_5 + 9 Cu → 5 Cu_3Sn). Meanwhile, these additional diffused Cu atoms can also further lead Sn atoms to be separated from Cu_6Sn_5 phase for an incomplete reaction, i.e. Cu_6Sn_5 + Cu → Cu_3Sn + Sn. Then, Sn atoms are migrating toward to the Cu_3Sn layer or copper substrates. Thereby, the reaction such as 6Cu + 5Sn → Cu_6Sn_5 may take place within the Cu_3Sn layer to a certain extent. This is the primary reason why a mixture of Cu_6Sn_5 and Cu_3Sn IMCs phases was formed and observed in the experiments above.

During this solid-solid reaction process, grain boundary diffusion is the predominant mechanism for transporting Cu and Sn atoms through the Cu_3Sn layer and diffusion in the Cu_6Sn_5 layer at the same time. Once the Cu atoms arrive at the interface of Cu_6Sn_5/Cu_3Sn, the reaction (Cu_6Sn_5 + 9 Cu → 5 Cu_3Sn) can be initiated immediately. On some occasions, the Cu atoms may be concentrated on the triple junctions of Cu_6Sn_5 grains by transporting through grain boundaries which act as channels. When the concentration of Cu is high enough at the triple junctions, the reaction can also occur to form Cu_3Sn locally within Cu_6Sn_5 IMC layer, as shown in Fig. 11 (b, c). Nevertheless, due to the shortened diffusing distance, the reaction on these locations in adjacent to Cu_6Sn_5/Cu_3Sn interface is much quicker compared to the places away from interface. Thus, this explains the observation encountered, i.e. with the increase of dwell time, the thickness of Cu_6Sn_5 layers is decreased while the increase of Cu_3Sn layer is taking the planar growth behavior. If the IMCs interlayer is thick enough, the microstructure of Cu_6Sn_5 will be different, as illustrated in Fig. 11 (d). Because the ripening of grains is expected to proceed throughout the whole soldering process, the Cu_6Sn_5 grains are likely to be single crystals in the perpendicular direction bridging the upper and lower Cu substrates. This kind of microstructure has been observed in Zhang's experiment [24, 28].

In addition, a second Cu_3Sn layer (Cu_3Sn-II) has formed between the Cu_3Sn-I layer and Cu substrate, constituting of ultra-fine grains. It is attributed by the numerous grain boundaries existing in the electroplated Cu layer due to the formation of finer grains, which can subsequently act as many nucleation sites to accelerate the Cu-Sn reaction. Thus, the number of Cu_3Sn-II grains can dramatically increase, but unable to grow up under the restricted available spaces. Then, the Cu_3Sn-II layer is constituted with equiaxial-grains which has been observed in the experiment. With the dwell time increasing, the Cu_3Sn-II layer can grow thicker and become more continuous towards the electroplated copper substrate. Meanwhile, the diffusion rate of Sn atoms is much slower than the rate of Cu in the Cu_3Sn layer [29], as such the Kirkendall voids are expected to present as the vacancies left behind the migration of Cu atoms. And, the volume contraction occurs during formation of the IMCs is approximately 7% for the Cu-Sn system [30], which may be the other cause contributing to the voids formation in the Cu_3Sn-II layer and Cu_3Sn-I layer.

After completion of the reactions, there will be primarily Cu_3Sn IMC remained at the interconnected joint as presented by Fig. 11 (e-f). The Cu_3Sn grains are more likely to be equiaxial shape, which are mixed with some Cu_6Sn_5 grains surrounding the coarse Cu_3Sn grains. Together with the analysis about gain size of Cu_3Sn IMC shown in Fig. 7, the ripening of Cu_3Sn grains can proceed as dwell time increases. Since the steepest concentration gradient of Cu atoms is along the vertical direction, which will fundamentally affect the diffusion controlled ripening process in Cu_3Sn layer. Thus, the grain of Cu_3Sn IMC can propagate to be columnar shape when the ripening process of Cu_3Sn grains is completed as shown in Fig. 11 (f).

3.4 Mechanical testing by Nano-indentation

A micropillar made by FIB from the sample formed with 70 minutes dwell time has been tested to observe the fracture surfaces after shearing by Nanoindentation. The results are shown in Fig. 12 (a) and (b), from which, the details of fracture can be manifested in the enlarged images. The fractured surface on the porous Cu_3Sn presents numerous micro-voids, taking both convex and concave profiles as seen in Fig. 12 (c). On the opposite fractured surface in Fig. 12 (d), it is not surprised to see that voids are also distributed inside the IMC uniformly, and some steps due to the fracture at different height, as well as some intact grains can be clearly seen. This implies that both intergranular and transgranular fractures occurred simultaneously. In addition, the concave formed matches with the convex site on the opposite fracture surface.

From the profile of load versus depth recorded in Fig. 13, the ultimate shear strength was calculated from the maximum loading force divided by the actual fractured area, which is approximately 176MPa. This is much less than the calculated strength of single-crystal Cu_3Sn [31], but it is two times higher than the value from Lee's work [32]. This drastic increase in strength can be attributed by the existence of finer grains of the Cu_3Sn layer, through the mechanism known as fine-grain strengthening [33]. Besides, considering the low loading rate applied, there were enough time left for the crack propagating along adjacent grain facets, then, the Brittle Intergranular Fracture (BIF) [34] occurred. Also, the interlocking effect among these multi-prismatic grains can further increase the shear strength, which tends to be ignored in the conventional solder joints with relative larger size grains and tested under higher loading rate.

4. Conclusions

The results obtained from the experiments revealed the phase transformation process from Cu_6Sn_5 to Cu_3Sn with the increases of dwell time at the given temperature of 533K. It was found that the Cu_6Sn_5 grains initially formed at the interfaces of joints have been consumed gradually and subsequently converted into Cu_3Sn grains, and became a single Cu_3Sn IMC interconnection under the sufficient dwell time. There were two layers of Cu_3Sn IMC growing continuously from both sides of copper substrates and they continue to grow merging each other along the central line of the IMC joint. Meanwhile, Cu_6Sn_5 phase was seen to surround the Cu_3Sn phase at the beginning of phase transformation. On the basis of the grain-boundary diffusion mechanism, the growth process and ripening of Cu_3Sn grains can take place simultaneously with the depletion of Cu_6Sn_5 phase in the IMCs layer of the joints. And finally, the Cu_3Sn grains tend to take columnar shape in perpendicular to the interface of IMC/Cu substrate.

The microvoids were formed and observed in the Cu_3Sn layer due to the interfacial reactions in adjacent to the electroplated copper layer. It is worth of noticing that there was a second Cu_3Sn thin layer with ultra-fine equiaxial grains formed between the first Cu_3Sn layer and electroplated copper layer. This phenomenon was not been observed on the opposite side of interconnections near the oxygen-free rolled copper substrate. In addition, the results derived from the shear test by Nanoindentation indicate a relatively high shear strength of the IMC joints, though it involved with the porous Cu_3Sn layer. It has been found

that both intergranular and transgranular fracture have occurred, which may reflect the implications of different fracture mechanisms at different locations.

Acknowledgements

This research is funded through LU-HUST joint research degree program, and financially supported by a Marie Curie International Research Staff Exchange Scheme Project within the 7th European Community Framework Program, No. PIRSES-GA-2010-269113, entitled “Micro-Multi-Material Manufacture to Enable Multifunctional Miniaturized Devices (M6)” and a China-European Union technology cooperation project, No. 1110. The authors also acknowledge the research funding by the National Nature Science Foundation of China (NSFC) and The Research Grants Council (RGC) Joint Research project (NSFC NO. No. 61261160498, RGC NO.CityU101/12).

References

[1] K.N. Tu, H.Y. Hsiao, and C. Chen. Transition from flip chip solder joint to 3D IC microbump: Its effect on microstructure anisotropy. *Microelectron Reliab*, 2013, 53(1): p. 2-6.

[2] R. Dunne, Y. Takahashi, K. Mawatari, M. Matsuura, T. Bonifield, P. Steinmann, and D. Stepniak. Development of a stacked WCSP package platform using TSV (Through Silicon Via) technology. *Proceeding of the 62nd Electronic Components and Technology Conference (ECTC)*, San Diego, 2012, p. 1062-1067.

[3] P. Ramm, M.J. Wolf, A. Klumpp, R. Wieland, B. Wunderle, B. Michel, and H. Reichl. Through silicon via technology - processes and reliability for wafer-level 3D system integration. *Proceeding of the 58th Electronic Components and Technology Conference (ECTC)*, Lake Buena Vista, 2008, p. 841-846.

[4] M.Y. Guo, C.K. Lin, C. Chen, and K.N. Tu. Asymmetrical growth of Cu_6Sn_5 intermetallic compounds due to rapid thermomigration of Cu in molten SnAg solder joints. *Intermetallics*, 2012, 29(0): p. 155-158.

[5] M.S. Park, M.K. Stephenson, C. Shannon, L.A. Cáceres Díaz, K.A. Hudspeth, S.L. Gibbons, J. Muñoz-Saldaña, and R. Arróyave. Experimental and computational study of the morphological

evolution of intermetallic compound (Cu_6Sn_5) layers at the Cu/Sn interface under isothermal soldering conditions. *Acta Mater*, 2012, 60(13-14): p. 5125-5134.

[6] I.E. Anderson, and J.L. Harringa. Elevated temperature aging of solder joints based on Sn-Ag-Cu: Effects on joint microstructure and shear strength. *J Electron Mater*, 2004, 33(12): p. 1485-14496.

[7] R. Labie, W. Ruythooren, and J.V. Humbeeck. Solid state diffusion in Cu-Sn and Ni-Sn diffusion couples with flip-chip scale dimensions. *Intermetallics*, 2007, 15(3): p.396-403.

[8] H. Liu, K. Wang, K.E. Aasmundtveit, and N. Hoivik. Intermetallic Compound Formation Mechanisms for Cu-Sn Solid–Liquid Interdiffusion Bonding. *J Electron Mater*, 2012, 41(9): p. 2453-2462.

[9] J.F. Li, P.A. Agyakwa, and C.M. Johnson. Interfacial reaction in Cu/Sn/Cu system during the transient liquid phase soldering process. *Acta Mater*, 2011, 59(3): p. 1198-1211.

[10] E. Lugscheider, S. Ferrara, H. Janssen, A. Reimann, and B. Wildpanner. Progress and developments in the field of materials for transient liquid phase bonding and active soldering processes. *Microsyst. Technol*, 2004, 10(3): p. 233-236.

[11] T.T. Luu, A. Duan, K. Wang, K. Aasmundtveit, and N. Hoivik. Cu/Sn SLID wafer-level bonding optimization. *Proceeding of the 63rd Electronic Components and Technology Conference (ECTC)*, Las Vegas, 2013, p. 1531-1537.

[12] N. Hoivik, K. Wang, K. Aasmundtveit, G. Salomonsen, A. Lapadatu, G. Kittilsland, and B. Stark. Fluxless wafer-level Cu-Sn bonding for micro-and nanosystems packaging. *Proceeding of the 3rd Electronic System-Integration Technology Conference (ESTC)*, Berlin, 2010, p. 1-5.

[13] N. Bosco, and F. Zok. Critical interlayer thickness for transient liquid phase bonding in the Cu-Sn system. *Acta Mater*, 2004, 52(10): p. 2965-2972.

[14] X.Q. Lin, and L. Luo. Void Evolution in Sub-100-Micron Sn-Ag Solder Bumps during Multi-reflow and Aging and its Effects on Bonding Reliability. *J Electron Mater*, 2008, 37(3): p. 307-313.

[15] D. Kim, J.H. Chang, J. Park, and J.J. Pak. Formation and behavior of Kirkendall voids within intermetallic layers of solder joints. *J Mater Sci Mater Electron*, 2011, 22(7): p. 703-716.

[16] K. Zeng, R. Stierman, T.C. Chiu, D. Edwards, K. Ano, and K.N. Tu. Kirkendall void formation in eutectic SnPb solder joints on bare Cu and its effect on joint reliability. *J Appl Phys*, 2005, 97(2): p. 024508.

[17] G. Ghosh. Elastic properties, hardness, and indentation fracture toughness of intermetallics relevant to electronic packaging. *J Mater Res,* 2004, 19(05): p.1439-1454.

[18] C.C. Lee, P.J. Wang, and J.S. Kim. Are intermetallics in solder joints really brittle? *Proceeding of the 57th Electronic Components and Technology Conference (ECTC),* Reno, 2007, p. 648-652.

[19] S.J. Wang, L.H. Hsu, N.K. Wang, and C.E. Ho. EBSD Investigation of Cu-Sn IMC microstructural evolution in Cu/Sn-Ag/Cu microbumps during isothermal annealing. *J Electron Mater* 2014, 43(1): p. 219-228.

[20] N. Mookam, and K. Kanlayasiri. Evolution of intermetallic compounds between Sn-0.3Ag-0.7Cu low-silver lead-free solder and Cu substrate during thermal aging. *J Mater Sci Technol*, 2012, 28(1): p. 53-59.

[21] S.H. Kim, and J. Yu. Secondary IMC formation induced by Kirkendall voiding in Cu/Sn-3.5Ag solder joints. *J Mater Res,* 2010, 25(09): p. 1854-1858.

[22] P.J. Shang, Z.Q. Liu, X.Y. Pang, D.X. Li, and J.K. Shang. Growth mechanisms of Cu_3Sn on polycrystalline and single crystalline Cu substrates. *Acta Mater,* 2009, 57(16): p. 4697-4706.

[23] A. Paul, C. Ghosh, and W.J. Boettinger. Diffusion parameters and growth mechanism of phases in the Cu-Sn system. *Metall Mater Trans A,* 2011, 42(4): p. 952-963.

[24] R. Zhang, Y. Tian, C. Hang, B. Liu, and C. Wang. Formation mechanism and orientation of Cu_3Sn grains in Cu-Sn intermetallic compound joints. *Mater Lett,* 2013, 110(0): p. 137-140.

[25] V.V. Slezov, and V.V. Sagalovich. Diffusive decomposition of solid solutions. *Sov Phys Usp*, 1987, 30(1): p. 23-45.

[26] A.M. Gusak, and K.N. Tu. Kinetic theory of flux-driven ripening. *Phys Rev B*, 2002, 66(11): p. 115403.

[27] M. Elsey, S. Esedoglu, and P. Smereka. Simulations of anisotropic grain growth: Efficient algorithms and misorientation distributions. *Acta Mater,* (2013, 61(6): p. 2033-2043.

[28] C. Hang, Y. Tian, R. Zhang, and D. Yang. Phase transformation and grain orientation of Cu-Sn intermetallic compounds during low temperature bonding process. *J Mater Sci Mater Electron*, 2013, 24(10): p. 3905-3913.

[29] F. Gao, and J. Qu. Calculating the diffusivity of Cu and Sn in Cu3Sn intermetallic by molecular dynamics simulations. *Mater Lett*, 2012, 73(0): p. 92-94.

[30] S. Bader, W. Gust, and H. Hieber. Rapid formation of intermetallic compounds interdiffusion in the Cu-Sn and Ni-Sn systems. *Acta Metall Mater*, 1995, 43(1): p. 329-337.

[31] H. Cheng, C. Yu, and W. Chen. Strain- and strain-rate-dependent mechanical properties and behaviors of Cu_3Sn compound using molecular dynamics simulation. *J Mater Sci*, 2012, 47(7): p. 3103-3114.

[32] B. Lee, J. Park, S. Jeon, K. Kwon, and H. Lee. A Study on the Bonding Process of Cu Bump/Sn/Cu Bump Bonding Structure for 3D Packaging Applications. *J Electrochem Soc*, 2010, 157(4): p. H420-H424.

[33] N. Hansen. Hall-Petch relation and boundary strengthening. *Scripta Mater*, 2004, 51(8): p. 801-806.

[34] M. Grah, K. Alzebdeh, P.Y. Sheng, M.D. Vaudin, K.J. Bowman, and M. Ostoja-Starzewski. Brittle intergranular failure in 2D microstructures: Experiments and computer simulations. *Acta Mater*, 1996, 44(10): p. 4003-4018.

Figure

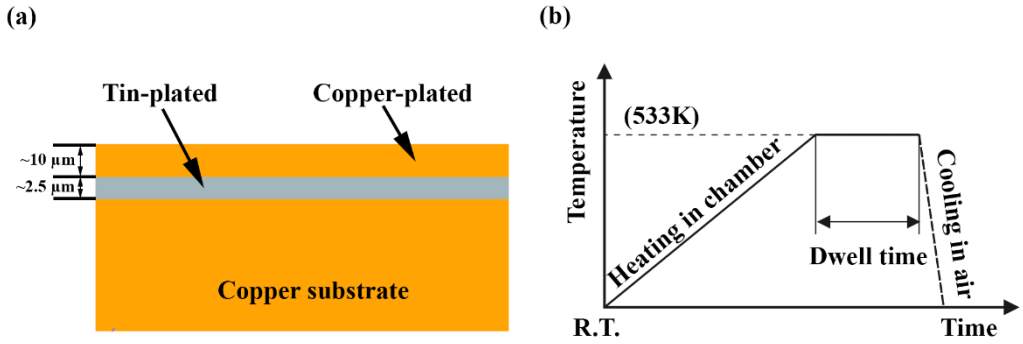

Fig. 1 Schematic diagram: (a) Cu/Sn/Cu sandwich structure made by electroplating; (b) the profile for preparing the Cu_3Sn IMC joints in vacuum chamber

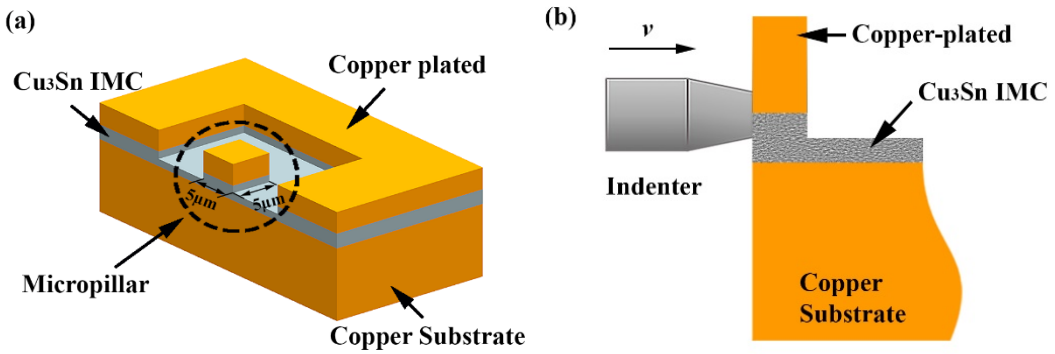

Fig. 2 Schematic illustration: (a) Testing micropillar fabricated by Focused Ion Beam (FIB); (b) Mechanical testing on micropillar by Nano-indenter

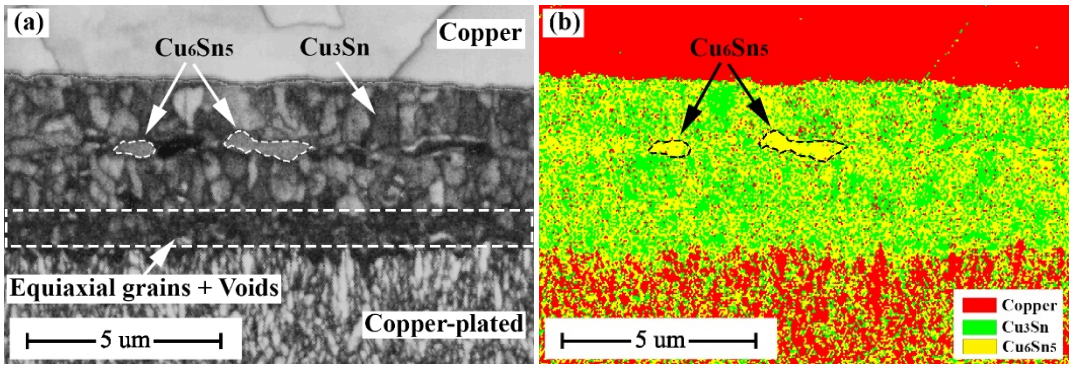

Fig. 3 EBSD images of the cross section of TLP bonded Cu/Sn/Cu interconnection with 10mins dwell time at 533K (a) IQ map (b) Phase map

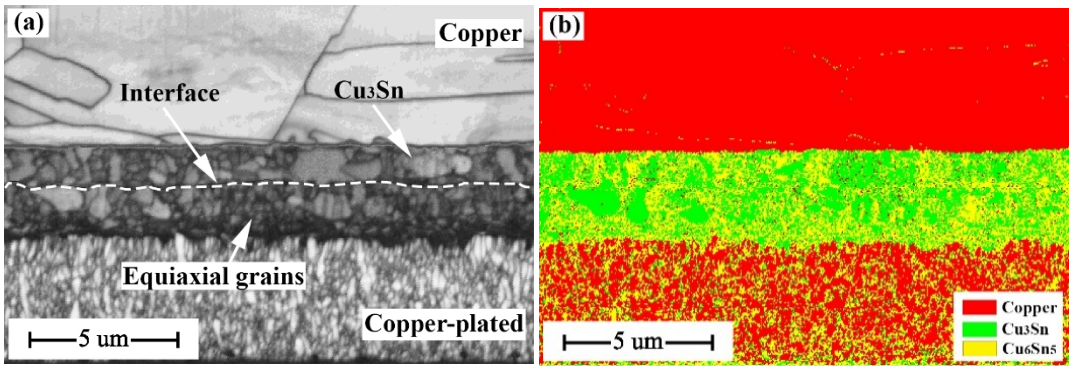

Fig. 4 EBSD images of the cross section of TLP bonded Cu/Sn/Cu interconnection with 30mins dwell time at 533K (a) IQ map (b) Phase map

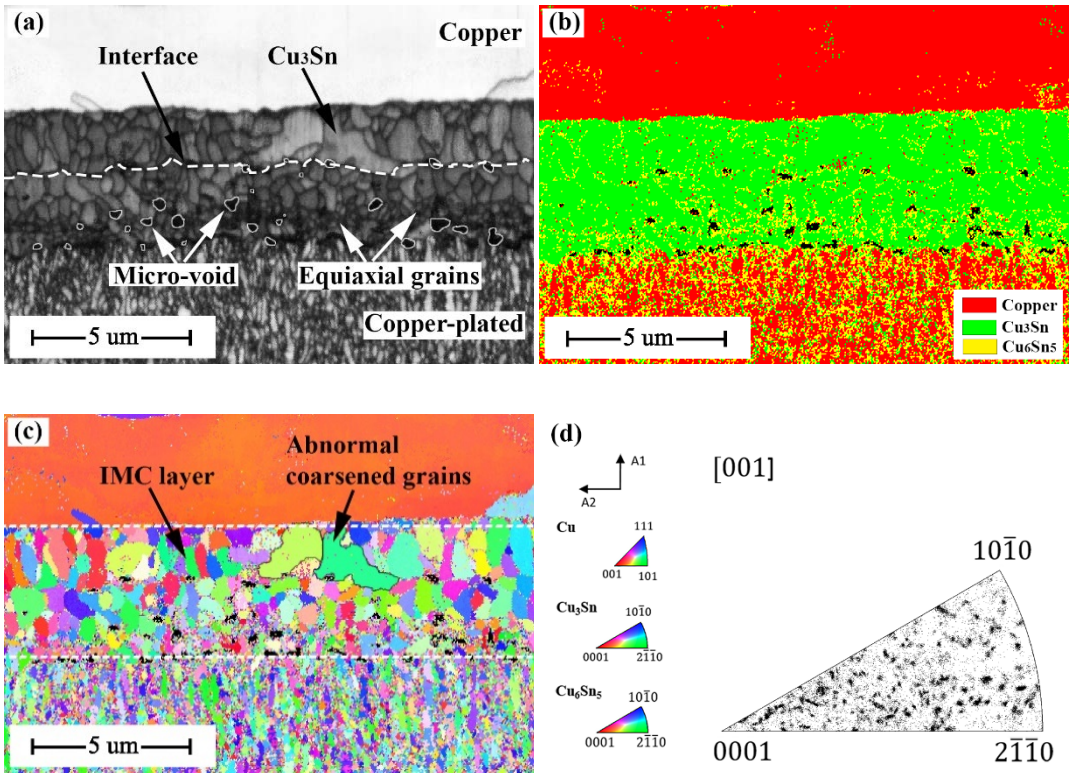

Fig. 5 EBSD images of the cross section of TLP bonded Cu/Sn/Cu interconnection with 70mins dwell time at 533K (a)IQ map (b)Phase map (c)IPF map (A1: Rotation direction and A2: Transverse direction) color codes are given in (d-left) and together with the discrete IPF of Cu_3Sn (d-right)

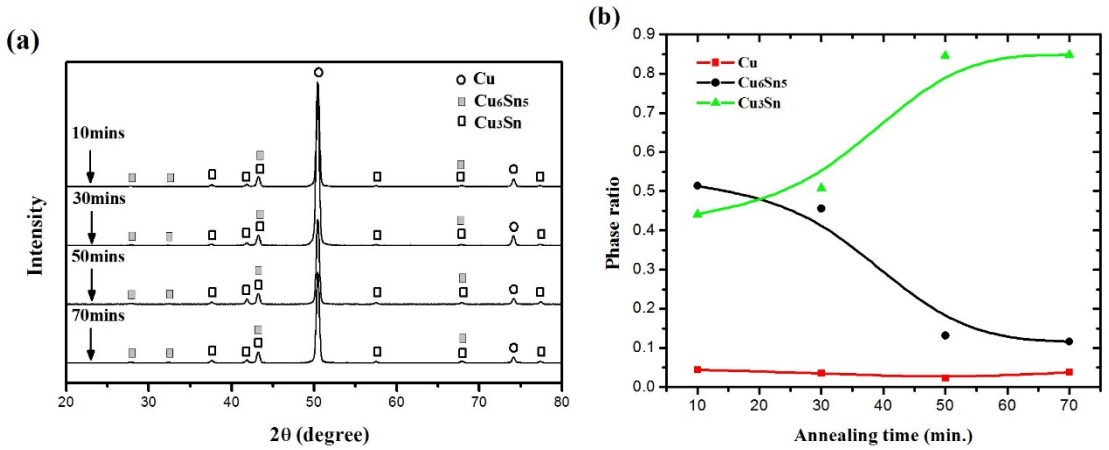

Fig. 6 (a) the XRD result of the IMCs interlayer and (b) the ratio of each phase in the IMCs interlayer of micro-joints changed with dwell time

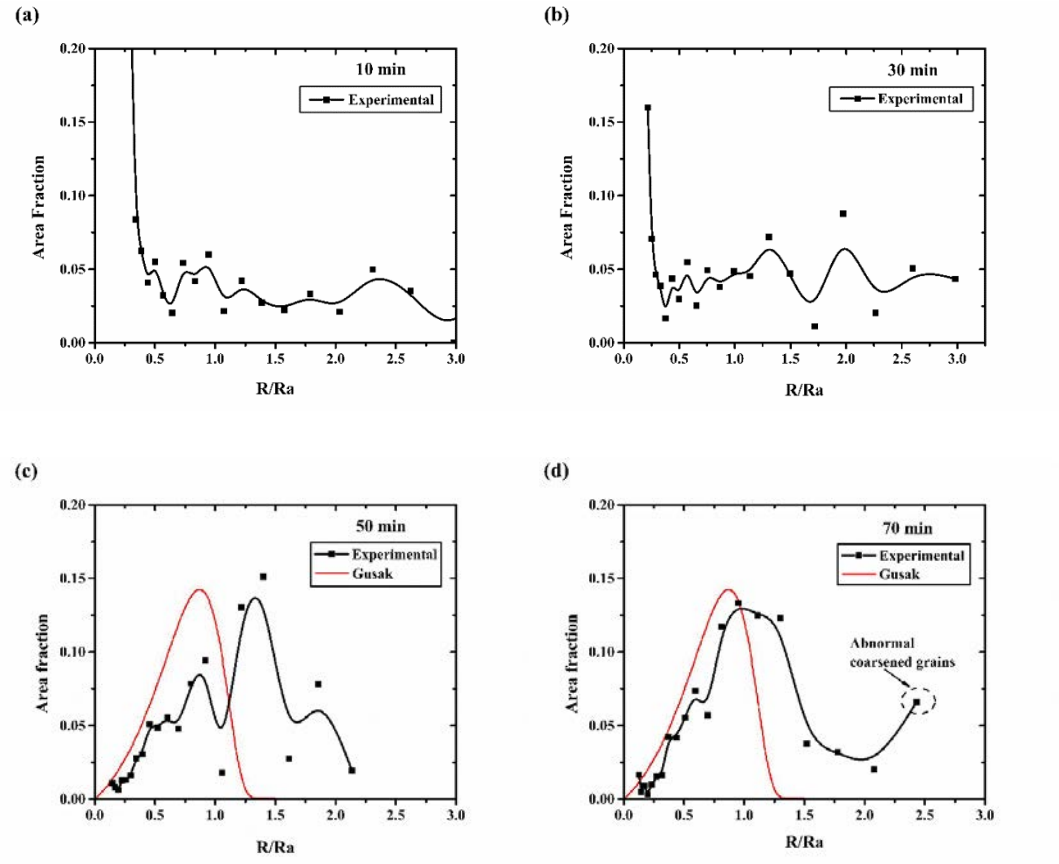

Fig. 7 Normalized grain size distribution of IMC interlayer formed at 533K as dwell time increases (a) 10mins, (b) 30mins, (c) 50mins, and (d) 70mins

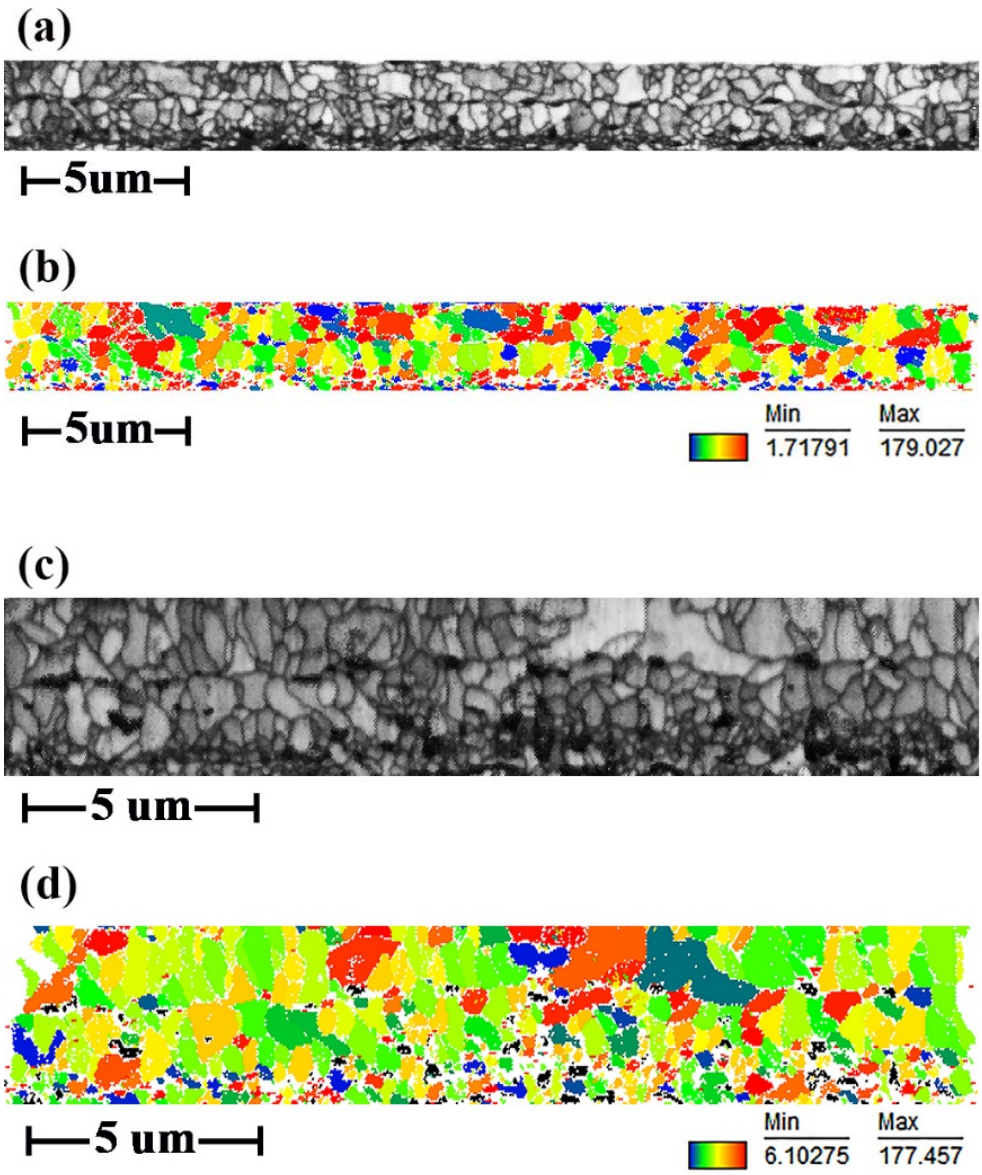

Fig. 8 EBSD images of Cu_3Sn IMC interlayer formed at dwell time of 50 mins: (a) IQ map, (b) GSO map; and 70 mins: (c) IQ map, (d) GSO map

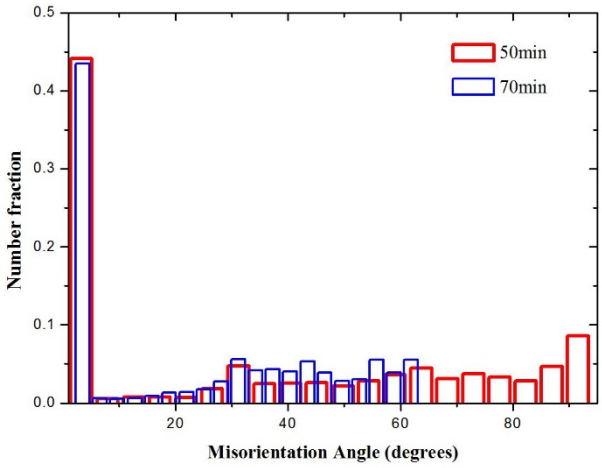

Fig. 9 Statistical results of misorientation distribution of IMC grains after aged for 50mins and 70mins

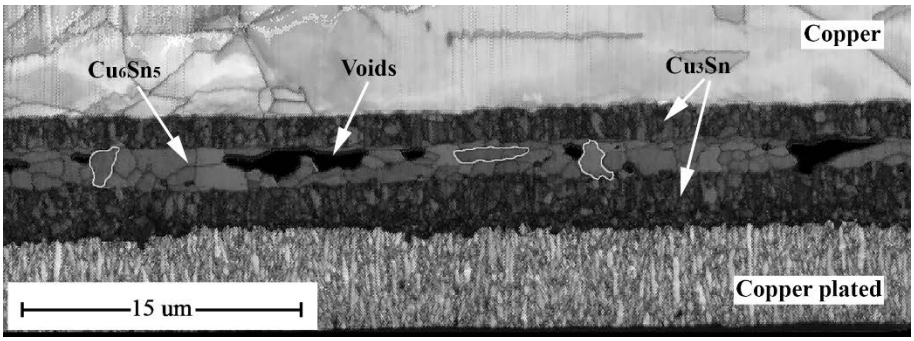

Fig. 10 IQ map on cross-section of TLP soldered Cn/~5μm Sn/Cu sandwich structure

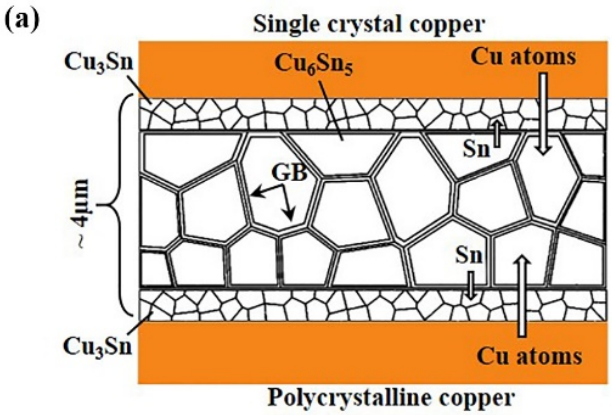

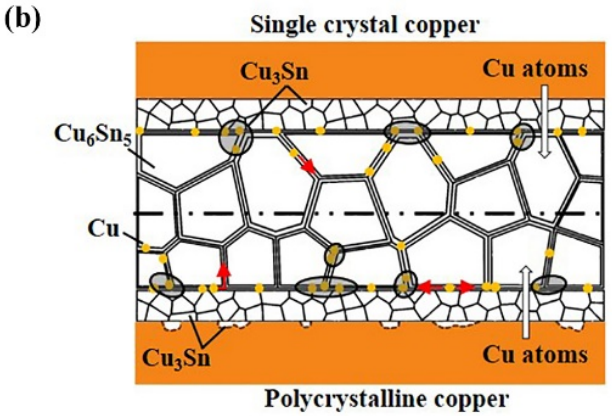
(b)
Single crystal copper
Cu3Sn
Cu atoms
Cu6Sn5
Cu
Cu3Sn
Cu atoms
Polycrystalline copper

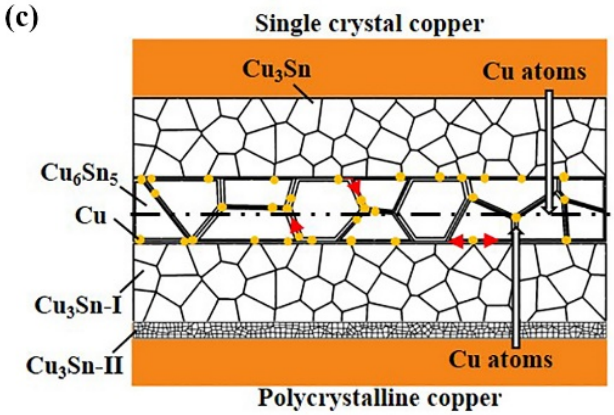
(c)
Single crystal copper
Cu3Sn
Cu atoms
Cu6Sn5
Cu
Cu3Sn-I
Cu3Sn-II
Cu atoms
Polycrystalline copper

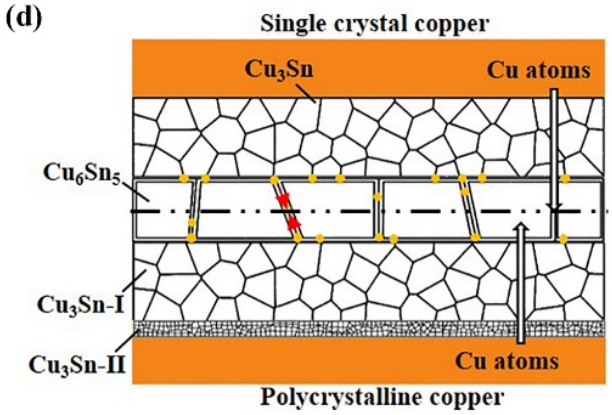
(d)
Single crystal copper
Cu3Sn
Cu atoms
Cu6Sn5
Cu3Sn-I
Cu3Sn-II
Cu atoms
Polycrystalline copper

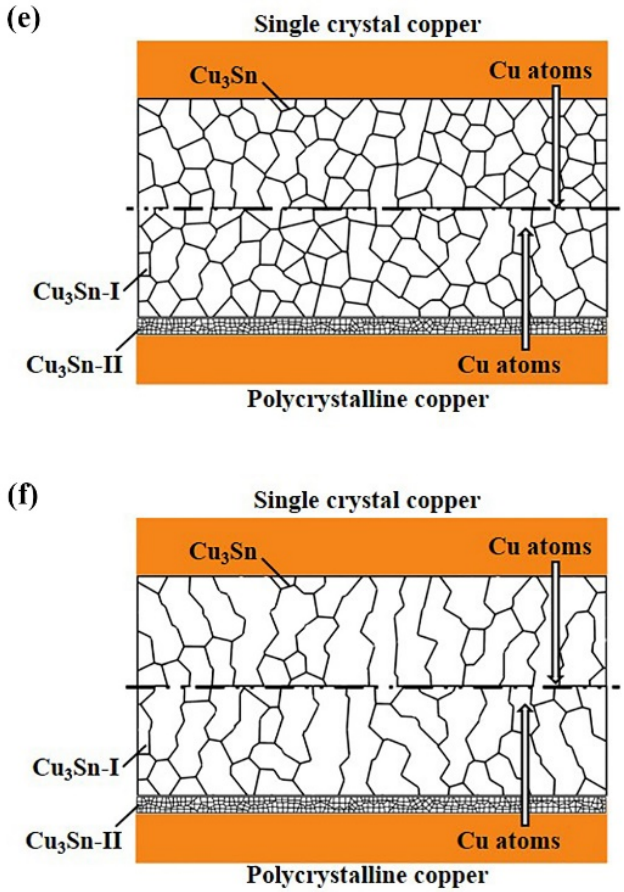

Fig. 11 The schematic diagram to ascribe the microstructural evolution process of Cu_6Sn_5 grains in the course of transformation into Cu_3Sn grains: (a) the initial IMCs joints formed; (b) the Cu atoms (yellow dots) diffuse from copper substrate into Cu_6Sn_5 layer through GB and concentrate on the triple junction forming Cu_3Sn grains; (c) with aging time increasing, the Cu_6Sn_5 layer in the middle consumed while the Cu_3Sn layers grow thicker, and the Cu_3Sn-II layer become continuous, mixing with some micro-voids; (d) another possible route similar to (c) for the Cu_6Sn_5 layer to propagate from (b), but through single crystal vertically; (e) complete Cu_3Sn formed in the joint; (f)the ripening of Cu_3Sn grains controlled by flux diffusion mechanism

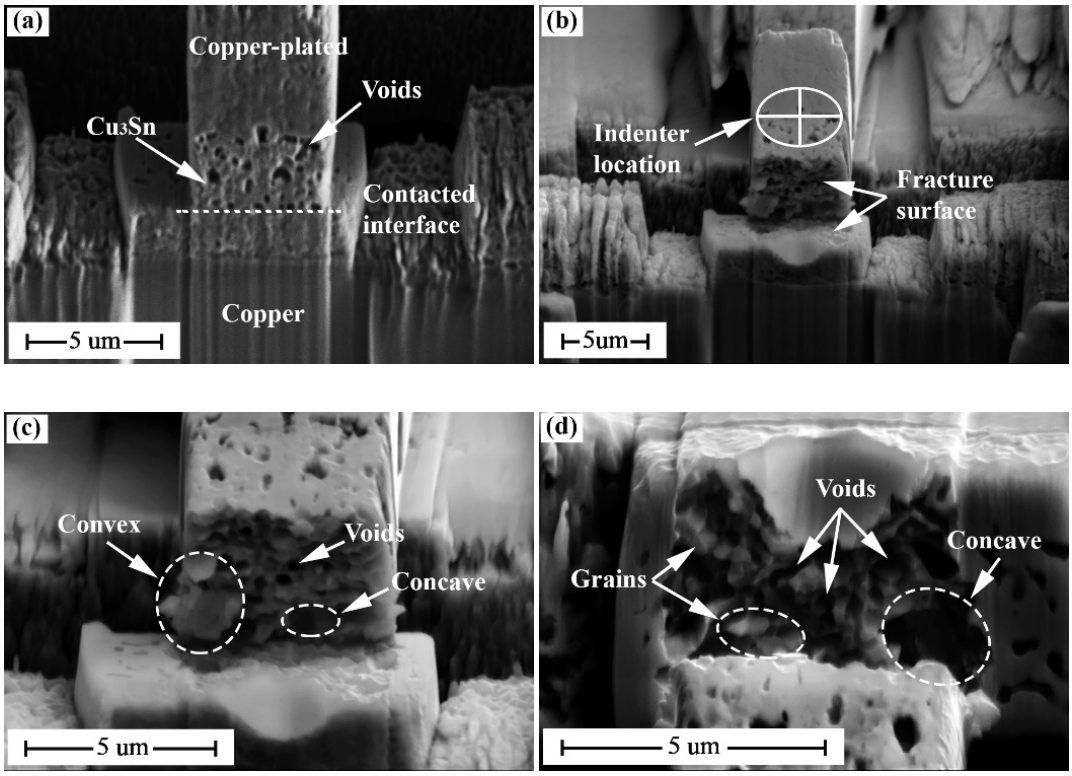

Fig. 12 SEM images of micropillar made by FIB before and after sheared by Nano-indentation (a) the micropillar before test; (b) indenter location and micropillar after test; (c) the upside fracture surface; (d)the downside fracture surface

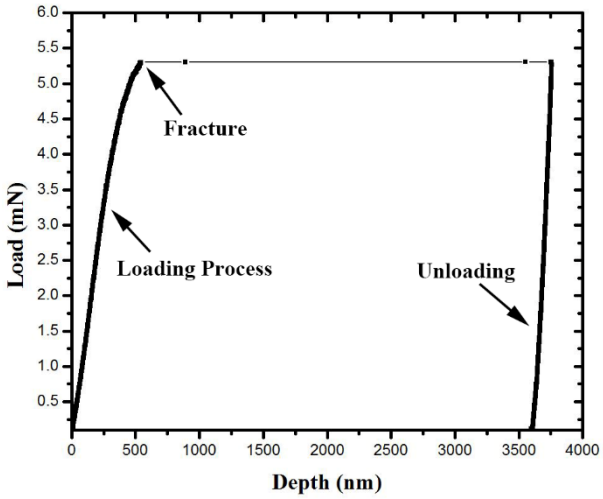

Fig.13 Load-depth curve during the shear testing by Nanoindentation